Proceedings of the 12th Workshop on Quantum Chaos and Localisation Phenomena (CHAOS 25)

Do Isoscattering Graphs Must Have the Same Eigenvalues?

M. Ławniczak[a], O. Farooq[a], S. Bauch[a], P. Kurasov[b] and L. Sirko[a]

[a]*Institute of Physics, Polish Academy of Sciences, Aleja Lotników 32/46, 02-668 Warszawa, Poland*
[b]*Department of Mathematics, Stockholm University, 106 91 Stockholm, Sweden*

Doi: 10.12693/APhysPolA.148.S9 *e-mail: lawni@ifpan.edu.pl

Our study focuses on isoscattering quantum graphs and their eigenvalues. Contrary to the prevailing assumption that isoscattering graphs are isospectral, we present a new example of non-isospectral isoscattering graphs and study their properties. Additionally, we expanded our research to include dissipative graphs that can be realized and studied experimentally using microwave networks.

topics: quantum graphs, M-function, isoscattering graphs, isospectral graphs

1. Introduction

The inverse problem is a key issue in many fields of physics and other sciences [1–4]. Reconstructing systems based on observations of their behavior (emission, scattering) is a great challenge for physicists and mathematicians. Quantum graphs, due to their relative simplicity and very well-developed mathematical methods describing them, are excellent tools for studying matters related to spectral inverse problems [5–9]. Another important feature of quantum graphs is the ability to simulate them using microwave networks, which allows for experimental verification of theoretical findings [10–12].

Quantum graphs Γ are metric graphs, formed from one-dimensional edges connected at vertices, equipped with a self-adjoint Laplace operator $L(\Gamma) = -\mathrm{d}^2/\mathrm{d}x^2$ acting in the Hilbert space of square-integrable functions, and with certain vertex conditions [5]. It is common that standard vertex conditions (continuity and sum of normal derivatives equal zero) are used at the vertices. In this case, the Laplace operator on the graph is uniquely determined by the metric graph; it plays the same role as the Laplace–Beltrami operator on manifolds. One may refer to its spectrum as the spectrum of the (metric) graph. If the metric graph is formed by finitely many compact edges, then the spectrum of the graph is discrete and all eigenvalues are non-negative [5, 7].

It is worth noting that quantum graphs are the paradigm of quantum chaotic systems [13]. Their properties are very well characterized by the random matrix theory (RMT) ensembles, such as the Gaussian orthogonal ensemble (GOE) [14–16], the Gaussian unitary ensemble (GUE) [17–19], or the Gaussian symplectic ensemble (GSE) [20–23].

The spectral inverse problem for quantum graphs involves reconstructing the topology and geometry of the graph knowing its eigenvalues. It was shown by Gutkin–Smilansky [24] and Kurasov–Nowaczyk [25] that the reconstruction is possible in an unambiguous manner if the edge lengths (ℓ) of the graph are incommensurable. Opening graphs by attaching leads (semi-infinite edges) allows the computation of scattering matrices (poles/resonances). In this case, the inverse problem involves determining the topology and geometry of the graph using the scattering matrix or just its singularities (resonances). Despite the fact that metric graphs are generically uniquely reconstructable from the scattering matrix (for example, all graphs with rationally independent edge lengths), wide families of graphs with equal scattering matrices exist. (One may increase reconstructability of metric graphs by considering spectral data dependent on magnetic fluxes; this approach was proposed in [26] and accomplished in [7], but we do not consider magnetic fluxes in the current paper.)

As mentioned above, when the edge lengths are commensurable — for example, if some of their edges have equal lengths — then it is possible to find a pair of graphs having exactly the same spectrum, called isospectral. Looking at the scattering matrix, we call two graphs with the same scattering matrix isoscattering.

Relations between isoscattering and isospectral graphs were first discussed in [27], where notions of isopolar and isophasal graphs were introduced. Interesting connections between isospectral

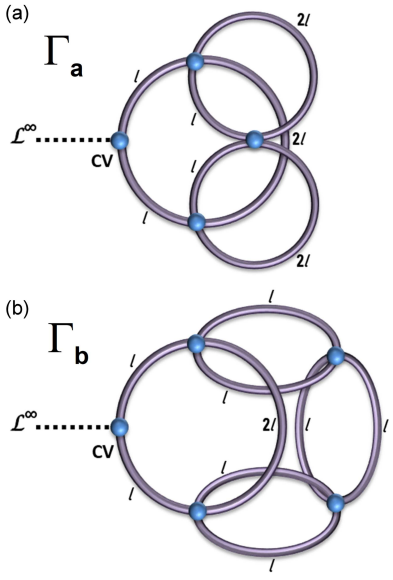

Fig. 1. Panels (a) and (b) show graphs Γ_a and Γ_b, respectively, with standard vertex conditions at all vertices and edge lengths indicated. Contact vertices are denoted as 'CV'. Each network is connected to an infinite lead, denoted as $\mathcal{L}^\infty$. The compact parts of both networks have the same total length $L_{tot} = 10\ell$.

and isoscattering graphs were discussed. Different kinds of symmetries played important roles in these examples. Until recently, experimental [28, 29] and numerical studies [27, 30, 31] dealt with multi-port variants of isoscattering graphs that were isospectral. A departure from this idea has been presented in [32], in which a transformation from non-isoscattering and non-isospectral graphs to isoscattering but non-isospectral graphs was demonstrated. In this article, we will present an analytical and numerical analysis of a pair of metric graphs, characterized by single-port scattering matrices that are isoscattering but not isospectral. In our studies, we shall always examine compact metric graphs formed by a finite number of compact edges and extended (non-compact) graphs obtained by attaching infinite leads to compact graphs. When we say that two graphs are isospectral, we mean that the compact parts have the same spectrum; when we say that two graphs are isoscattering, we mean that the extended graphs have the same scattering matrix. Physical intuition says that eigenvalues of the compact core should produce resonances of the scattering matrix associated with the extended graphs.

The Titchmarsh–Weyl M-functions [7] will be used as a powerful tool to identify isoscattering graphs and explain the reason for their isoscattering behavior. The existence of vertices of different graphs having equal M-functions is a necessary and sufficient condition for the extended graphs to be isoscattering.

2. Analytic approach

2.1. Strategy

Consider the two graphs presented in Fig. 1. We claim that:

- the extended graphs have the same scattering matrix, in other words, the Titchmarsh–Weyl M-functions associated with the contact vertices on the compact graphs coincide;
- the compact graphs are not isospectral.

The M-function is completely determined by the spectra of compact graphs and boundary values of the corresponding eigenfunctions at the contact vertices (see formula (17.26) in [7])

$$M_\Gamma(\lambda) = -\left(\sum_{n=1}^{\infty} \frac{\left\langle \psi_n^{\mathrm{st}}\big|_{\partial\Gamma}, \cdot \right\rangle_{\ell_2(\partial\Gamma)} \ \psi_n^{\mathrm{st}}\big|_{\partial\Gamma}}{\lambda_n^{\mathrm{st}} - \lambda}\right)^{-1}. \quad (1)$$

Here, λ_n^{st} are the eigenvalues of the standard Laplacian on a compact metric graph Γ, and ψ_n^{st} are the corresponding normalized eigenfunctions. The formula (1) explicitly shows that the M-functions are determined by the spectrum and the values of the eigenfunctions at the contact vertices. It takes a slightly simpler form in the case of a single contact vertex v_0, namely

$$M_\Gamma(\lambda) = -\left(\sum_{n=1}^{\infty} \frac{\left|\psi_n^{\mathrm{st}}(v_0)\right|^2}{\lambda_n^{\mathrm{st}} - \lambda}\right)^{-1}. \quad (2)$$

Only eigenfunctions that are not equal to zero at v_0 contribute to the M-function, i.e., if $\psi_n^{\mathrm{st}}(v_0) = 0$, then the corresponding eigenvalue is not a zero of the M-function (provided, of course, that there is no other eigenfunction with the same eigenvalue and non-zero value at v_0).

Thus, to prove that the graphs are isoscattering but not isospectral, it is enough to show that the graphs Γ_a and Γ_b are not isospectral, but the eigenfunctions with non-zero values at the contact vertex correspond to the same eigenvalues and have the same values at the contact vertex.

Our proof of these two statements will be based on internal symmetries of the two graphs. We proceed as follows:

(i) The two graphs are invariant under reflection J with respect to the horizontal lines. The eigenfunctions can be separated into symmetric and antisymmetric ones with respect to the reflection. We call this the first symmetry reduction.

(ii) Antisymmetric eigenfunctions are equal to zero at the contact vertices and therefore can be ignored when the M-function is calculated. Of course, these eigenfunctions should not be ignored when the spectra of the metric graphs are calculated to show their non-isospectrality.

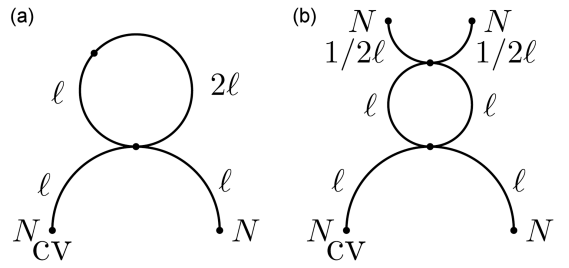

Fig. 2. The graphs $\Gamma_{a'}$ and $\Gamma_{b'}$ support symmetric eigenfunctions of the graphs Γ_a and Γ_b, respectively. Symbols used: N — Neumann boundary condition, CV — contact vertex.

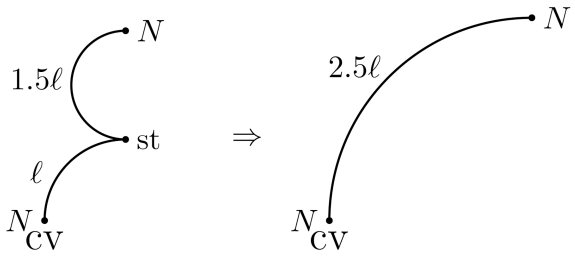

Fig. 3. Stretching of the graph preserves symmetric–symmetric eigenfunctions. Here, 'st' and N denote the standard and Neumann boundary conditions, respectively.

(iii) To calculate the symmetric eigenfunctions, it is enough to consider one of the two halves of the original graphs Γ_a and Γ_b. We denote these new graphs as $\Gamma_{a'}$ and $\Gamma_{b'}$ and present them in Fig. 2. The symmetric eigenfunctions on Γ_a and Γ_b can be restored from their values on the quotient graphs $\Gamma_{a'}$ and $\Gamma_{b'}$ using the symmetry.

Symmetric eigenfunctions automatically satisfy Neumann conditions at the intersection points between the symmetry axis and the metric graph. Hence, the restrictions of the eigenfunctions to the quotient graphs satisfy Neumann conditions at these vertices (having degree one). These conditions turn into standard conditions in the case of higher-degree vertices. We use the fact that two edges connected at a degree two vertex with standard conditions can be substituted by one longer edge as shown in Fig. 3.

(iv) Obtained quotient graphs are symmetric again, and we can repeat our trick, splitting the eigenfunctions into symmetric and antisymmetric ones, with the following important difference, namely that there is no reason for all antisymmetric eigenfunctions to be equal to zero at the contact vertex, since it does not belong to the symmetry axis of the quotient graphs.

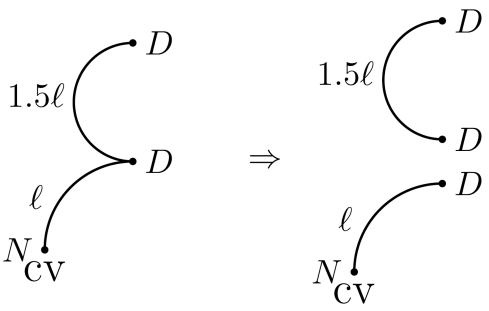

Fig. 4. Splitting of the graph preserves antisymmetric–symmetric eigenfunctions. Here, D and N denote the Dirichlet and Neumann boundary conditions, respectively.

In what follows, we shall adopt the following convention: the eigenfunctions, which are symmetric or antisymmetric with respect to the first symmetry, will be called simply symmetric and antisymmetric, respectively. The eigenfunctions that are in addition symmetric or antisymmetric with respect to the second symmetry will be indicated by adding the corresponding property in front. For example, an antisymmetric–symmetric eigenfunction is an eigenfunction that is symmetric with respect to the first symmetry and antisymmetric with respect to the second one.

2.2. The graphs are isoscattering

To prove that the graphs are isoscattering, we need to determine the spectra of the symmetric eigenfunctions and their values at the contact vertices for both graphs Γ_a and Γ_b. Using the symmetry of the mentioned graphs, we have already reduced the problem to finding the eigenfunctions for the reduced graphs $\Gamma_{a'}$ and $\Gamma_{b'}$. Now, using the symmetry of these graphs with respect to the vertical axis, we shall perform the second symmetry reduction, separately for each graph.

2.2.1. Symmetry reduction for the graph $\Gamma_{a'}$

The graph $\Gamma_{a'}$ is again invariant; this time under the reflection with respect to the vertical axis. Hence, all its eigenfunctions can be split into symmetric and antisymmetric (symmetric eigenfunctions). The symmetric–symmetric eigenfunctions coincide with the eigenfunctions of the graph given in Fig. 3.

Calculating antisymmetric–symmetric eigenfunctions, we obtain Dirichlet conditions at the intersections between the vertical axis and the graph $\Gamma_{a'}$ (see Fig. 4). The Dirichlet conditions at the middle

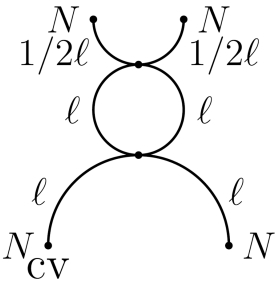

Fig. 5. The graph $\Gamma_{b'}$ supports symmetric eigenfunctions of the graph Γ_b.

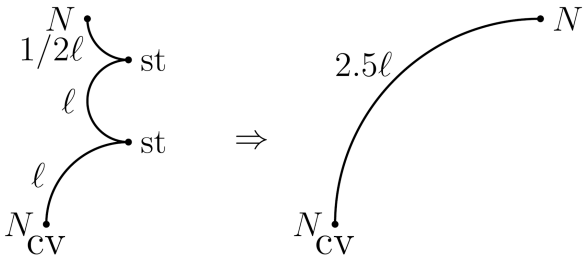

Fig. 6. Stretching of the graph preserves symmetric–symmetric eigenfunctions.

vertex split the graph into two independent graphs. Only eigenfunctions supported by the lower graph contribute to the M-function of $\Gamma_{a'}$ (and hence to the M-function of Γ_a). The antisymmetric–symmetric eigenfunctions supported by the upper graph are identically equal to zero near the contact vertex.

2.2.2. Symmetry reduction for the graph $\Gamma_{b'}$

The metric graph $\Gamma_{b'}$ supporting symmetric eigenfunctions for the graph Γ_b is presented in Fig. 5. As before, we use the symmetry of $\Gamma_{b'}$ and consider the eigenfunctions symmetric and antisymmetric with respect to the vertical axis.

The quotient graph supporting symmetric–symmetric eigenfunctions can be seen (as in the previous case) as the interval graph with Neumann conditions at both end points.

Figure 6 shows the quotient graph used to determine the symmetric–symmetric eigenfunctions of Γ'_b, with Neumann boundary conditions at both ends.

The quotient graph corresponding to antisymmetric–symmetric eigenfunctions has Dirichlet conditions at two vertices, which separate it into three non-connected metric graphs. Figure 7 presents this splitting of the graph carrying antisymmetric–symmetric eigenfunctions of Γ'_b, divided into three disconnected parts by the Dirichlet vertices.

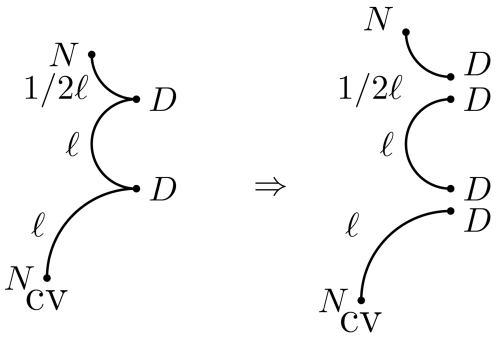

Fig. 7. Splitting of the graph preserves antisymmetric–symmetric eigenfunctions.

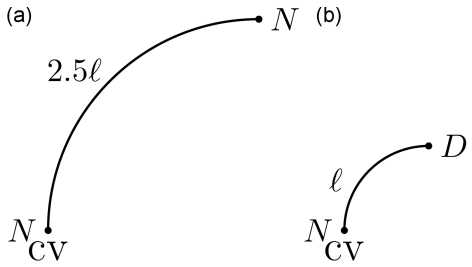

Fig. 8. The graphs whose eigenfunctions determine symmetric and antisymmetric–symmetric eigenfunctions of $\Gamma_{a'}$ and $\Gamma_{b'}$ contributing to the M-functions of Γ_a and Γ_b.

Only eigenfunctions supported by the graph shown in Fig. 4 contribute to the M-function of $\Gamma_{a'}$ (and hence to the M-function of Γ_a). This graph coincides with the graph supporting antisymmetric–symmetric eigenfunctions on $\Gamma_{a'}$ and contributing to the M-function. The antisymmetric–symmetric eigenfunctions supported by the two upper graphs are identically equal to zero near the contact vertex, and therefore do not contribute to the M-functions.

2.2.3. Sum up

We see that the graphs Γ_a and Γ_b have the same M-function determined by the eigenfunctions of the graphs presented in Fig. 8.

The corresponding eigenvalues $\lambda_n = k_n^2$ are as follows

$$\lambda_n = \begin{cases} \left(\dfrac{2\pi}{5\ell}n\right)^2, & n = 0, 1, 2\ldots, \\ \left(\dfrac{\pi}{\ell}\left(\dfrac{1}{2}+n\right)\right)^2, & n = 0, 1, 2\ldots. \end{cases} \tag{3}$$

The corresponding eigenfunctions coincide and therefore trivially have precisely the same values at the contact vertices. Formula (2) implies that the M-functions coincide.

2.3. The graphs are not isospectral

We have just calculated the common spectra of the two graphs corresponding to eigenfunctions, which are not equal to zero at the contact vertices. In what follows, we shall calculate the remaining eigenvalues, but we will start with the proof of the non-isospectrality of the presented graphs using their Euler characteristics.

2.3.1. Non-isospectrality via Euler characteristic

The easiest way to see that the graphs Γ_a and Γ_b are not isospectral is to look at their Euler characteristics [32–37], i.e.,

$$\chi(\Gamma_a) = V_a - E_a = 4 - 7 = -3,$$
$$\chi(\Gamma_b) = V_b - E_b = 5 - 9 = -4, \tag{4}$$

where V and E are the number of vertices and edges of these graphs. The Euler characteristic is uniquely determined by the spectrum $\lambda_n(\Gamma) = k_n^2$ (see [34, 35] or formula (9.1) in [7]), i.e.,

$$\chi(\Gamma) = 2 + 2 \lim_{t\to\infty} \sum_{k_n \neq 0} \cos(k_n/t) \left[\frac{\sin(k_n/2t)}{k_n/2t}\right]^2. \tag{5}$$

Two isospectral graphs, in fact, must have the same Euler characteristic; however, the graphs Γ_a and Γ_b do not.

2.3.2. Symmetric eigenfunctions

We start with symmetric eigenfunctions on Γ_a and Γ_b. We need to examine just the eigenfunctions that are equal to zero at the contact vertices. These eigenfunctions are the eigenfunctions supported by graph in Fig. 4 for $\Gamma_{a'}$ and the eigenfunctions supported by the two graphs in Fig. 7 for $\Gamma_{b'}$.

For the first graph, these eigenvalues coincide with the Dirichlet–Dirichlet eigenvalues on the interval of length 1.5ℓ, thus

$$\lambda_n = \left(\frac{\pi}{1.5\ell} n\right)^2, \quad n = 1, 2, \ldots. \tag{6}$$

For the second graph, these eigenvalues coincide with the Dirichlet–Dirichlet eigenvalues of the interval of length ℓ and Dirichlet–Neumann eigenvalues of the interval of length $\frac{1}{2}\ell$, thus

$$\lambda_n = \begin{cases} \left(\frac{\pi}{\ell} n\right)^2, & n = 1, 2, \ldots, \\ \left(\frac{\pi}{\ell}(1+2n)\right)^2, & n = 0, 1, 2, \ldots. \end{cases} \tag{7}$$

We see that these spectra are different, but to complete our study, we need to prove that antisymmetric eigenfunctions on Γ_a and Γ_b cannot compensate for the non-isospectrality.

2.3.3. Antisymmetric eigenfunctions

Antisymmetric eigenfunctions satisfy Dirichlet conditions at the intersections with the horizontal line. Figure 9 shows the quotient graphs $\Gamma_{a'}$ and $\Gamma_{b'}$ that support the antisymmetric eigenfunctions of Γ_a and Γ_b, respectively. Therefore, the same quotient graphs $\Gamma_{a'}$ and $\Gamma_{b'}$ can be used to calculate the antisymmetric eigenfunctions, but with Dirichlet vertex conditions at the vertices coming from the intersection points.

The quotient graphs are again symmetric with respect to the reflection in the vertical axis. The spectra determined by symmetric and antisymmetric eigenfunctions on the quotient graphs are determined by the equations presented below for:

- the graph $\Gamma_{a'}$
  - for symmetric–antisymmetric eigenfunctions
    We need to distinguish eigenfunctions that are equal to zero at the central vertex from those that are not. These equal to zero at the central vertex eigenfunctions are described by the equation
    $$\sin(k\ell) = 0. \tag{8}$$
    There are precisely two such eigenfunctions for each solution of the trigonometric equation (8), i.e., one equal to zero on the whole vertical axis and one equal to zero on the horizontal axis. As a result, we get the following spectral points
    $$\lambda = \left(\frac{2\pi}{\ell} n\right)^2, \tag{9}$$
    where $n = 1, 2, \ldots$, multiplicity two. The eigenfunctions equal to zero at the central vertex are described by
    $$3\cot(k\ell) + \cot(2k\ell) = 0 \Rightarrow \cos^2(k\ell) = \tfrac{1}{8}$$
    $$\Rightarrow \begin{cases} \lambda = \left[\frac{1}{\ell}\left(\arccos(\frac{1}{\sqrt{8}}) + \pi n\right)\right]^2, \\ \lambda = \left[\frac{1}{\ell}\left(\pi - \arccos(\frac{1}{\sqrt{8}}) + \pi n\right)\right]^2, \end{cases} \tag{10}$$
    where $n = 0, 1, 2, \ldots$;
  - for antisymmetric–antisymmetric eigenfunctions
    $$\sin(k\ell) = 0 \Rightarrow \lambda = \left(\frac{\pi}{\ell} n\right)^2, \tag{11}$$
    where $n = 1, 2, \ldots$;
- the graph $\Gamma_{b'}$
  - for symmetric–antisymmetric eigenfunctions
    $$\sin(2.5k\ell) = 0 \Rightarrow \lambda = \left(\tfrac{\pi}{2.5\ell} n\right)^2, \tag{12}$$
    where $n = 1, 2, \ldots$;

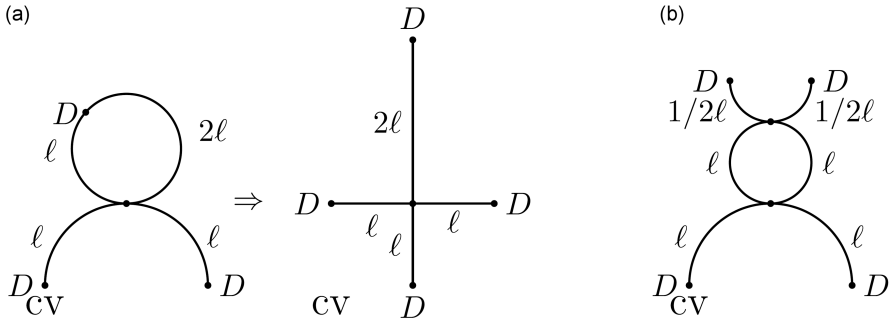

Fig. 9. The graphs $\Gamma_{a'}$ and $\Gamma_{b'}$ support antisymmetric eigenfunctions of the graphs Γ_a and Γ_b, respectively.

– for antisymmetric–antisymmetric eigenfunctions

$$\sin(k\ell) = 0 \Rightarrow \lambda = \left(\tfrac{\pi}{\ell} n\right)^2, \tag{13}$$

where $n = 1, 2, \ldots$, double eigenvalues, or

$$\sin(k\tfrac{\ell}{2}) = 0 \Rightarrow \lambda = \left(\tfrac{2\pi}{\ell} n\right)^2, \tag{14}$$

where $n = 1, 2 \ldots$.

Thus, the original graphs Γ_a and Γ_b are not isospectral.

2.4. Numerical results of analytical solutions

Let us consider graphs Γ_a and Γ_b with the total length $L_{tot} = 1$ m, and $\ell = 0.1$ m. In order to summarize our calculations of the spectra k_n of the graphs, we will constrain ourselves to a $\boldsymbol{k}$-vector range of 0 to 41.92 m^{-1}. In the context of a potential microwave realization of quantum graphs, this would require measuring the scattering matrix of microwave networks within the frequency range $f \in$ 0–2 GHz. The eigenvalues of k_n are presented in Table I. The eigenvalues of the non-zero functions at the contact vertices, whose equality means that graphs are isoscattering, are marked in bold.

Thus, we show analytically that the graphs Γ_a and Γ_b are isoscattering, have the same M-functions at contact vertices, but are not isospectral.

3. Numerical results

The scattering matrices $S(k) = |S(k)|e^{i\varphi}$ were calculated as a function of k for graphs Γ_a and Γ_b, as shown in Fig. 10. The core of the analysis involves computing the overall scattering matrix $\mathbb{S}$ for each graph and evaluating their reflection coefficients $S_{11}(k) = S(k)$. In the calculations, the pseudo-orbit method proposed by Exner and Lipovský [39, 40] was applied.

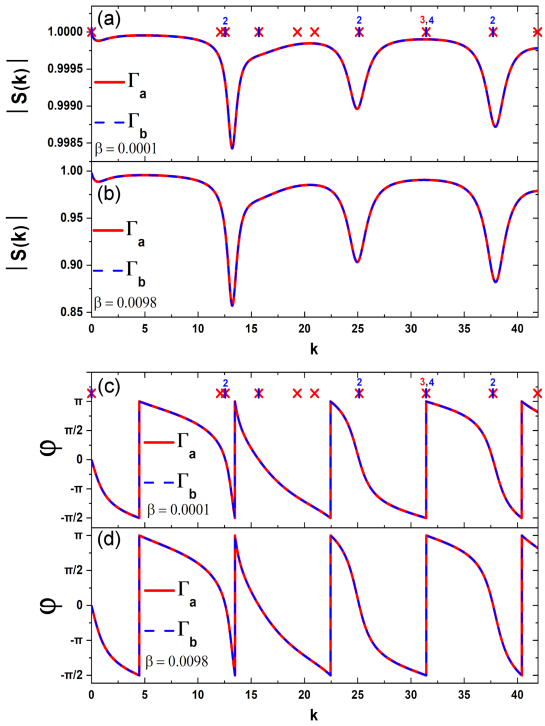

Fig. 10. Panels (a) and (c) and panels (b) and (d) show, respectively, the amplitudes $|S(k)|$ and the phases φ of the scattering matrices $S(k)$ calculated for the quantum graphs Γ_a (red solid line) and Γ_b (blue broken line). The calculations were performed in the $\boldsymbol{k}$-vector range of 0–41.92 m^{-1}. Different levels of dissipation are characterized by absorption coefficients $\beta = 0.0001$ and 0.0098 m$^{-1/2}$. The positions of the eigenvalues k_n are marked by red crosses and blue lines for Γ_a and Γ_b, respectively. The multiplicities of the eigenvalues that are different from 1 are marked by red and blue digits.

The propagation of an electromagnetic wave through a segment of a microwave network is governed by a complex wave vector $\kappa = k_r + ik_i$ [30]. The real part of κ is defined as $k_r = k = 2\pi f/c$, where c is the speed of light, and its imaginary component is given by $k_i = \beta\sqrt{k}$. In Fig. 10a and c

TABLE I

Eigenvalues k_n of graphs Γ_a and Γ_b in the interval $k \in 0$–41.92 m^{-1}.

Graph Γ_a											
0	12.09	**12.57**	**15.71**	19.32	20.94	**25.13**	31.41	31.41	31.41	**37.70**	41.88
Graph Γ_b											
0	12.57	**12.57**	**15.71**	25.13	**25.13**	31.41	31.41	31.41	31.41	**37.70**	37.70

and in Fig. 10b and d, we show, respectively, the amplitudes $|S(k)|$ and the phases φ of the scattering matrices $S(k)$ calculated for the quantum graphs Γ_a (red solid line) and Γ_b (blue broken line). As mentioned above, for practical reasons, we constrained our calculations to a $\boldsymbol{k}$-vector range of 0 to 41.92 m^{-1}. In the context of a potential microwave realization of quantum graphs, this would require measuring the scattering matrix of microwave networks within the frequency range $f \leq 2$ GHz. We investigated the effect of absorption on the system's response by performing simulations with two absorption coefficient values, i.e., $\beta = 0.0001$ m$^{-1/2}$ and $\beta = 0.0098$ m$^{-1/2}$.

The positions of the eigenvalues k_n presented in Table I are marked in Fig. 10 by red crosses and blue lines for Γ_a and Γ_b, respectively. The multiplicities of the eigenvalues that are different from 1 are marked by red and blue digits. It should be noted that eigenvalue $k = 31.42$, although common to both graphs, is not visible in the isoscattering spectra because the eigenfunctions corresponding to it are equal to zero at the CVs.

The agreement of the results of numerical calculations of the eigenvalues with the analytical results is very good. Only $k = 15.71$ for the graph Γ_a was not found.

A smaller value of the absorption coefficient β was chosen to demonstrate the strong dependence of $|S(k)|$ on β. For small β, the amplitude of the scattering matrix $|S(k)|$ is also very small. The larger value of β was selected to be close to the expected value in the microwave realization of quantum graphs. In this case, the amplitude of $|S(k)|$ is much larger, by an order of magnitude. For both values of the absorption coefficient β, the moduli of the scattering matrices $|S(k)|$ and the phases φ are perfectly overlapping, demonstrating that the graphs Γ_a and Γ_b are isoscattering. On the other hand, the graphs Γ_a and Γ_b are not isospectral, as is clearly shown by the calculated eigenvalues of the graphs.

4. Conclusions

The answer to the question posed in the title of this paper is negative. We have shown and studied the new example of non-isospectral isoscattering quantum graphs. Using the M-function formalism, we determined the conditions necessary for identifying and constructing these graphs. We validated our theoretical findings numerically by extending them to quantum graphs and microwave networks with dissipation.

References

[1] G. Lambaré, J. Virieux, R. Madariaga, S. Jin, *Geophysics* **57**, 1138 (1992).

[2] T. Marsh, *Astrophys. Space Sci.* **296**, 403 (2005).

[3] N.V. Shumakov, *Sov. Phys. Tech. Phys.* **2**, 771 (1957) (translated by American Institute of Physics).

[4] K. Chadan, P.C. Sabatier, R.G. Newton, *Inverse Problems in Quantum Scattering Theory*, 2nd ed., Springer Berlin, Heidelberg 2011.

[5] G. Berkolaiko, P. Kuchment, *Introduction to Quantum Graphs*, American Mathematical Society, 2013.

[6] P. Kuchment, *Proc. Symp. Pure Math.* **77**, 291 (2008).

[7] P. Kurasov, *Spectral Geometry of Graphs*, Birkhäuser, 2024.

[8] E.B. Davies, *J. Operator Theory* **69**, 195 (2013).

[9] V.A. Yurko, *Izv. Sarat. Univ. (N.S.) Ser. Mat. Mekh. Inform.* **21**, 343 (2021).

[10] O. Hul, S. Bauch, P. Pakoński, N. Savytskyy, K. Życzkowsk, L. Sirko, *Phys. Rev. E* **69**, 056205 (2004).

[11] M. Ławniczak, J. Lipovský, L. Sirko, *Phys. Rev. Lett.* **122**, 140503 (2019).

[12] T. Ghutishvili, L. Chen, S.M. Anlage, T.M. Antonsen, *Phys. Rev. Res.* **5**, 033195 (2023).

[13] T. Kottos, U. Smilansky, *Phys. Rev. Lett.* **79**, 4794 (1997).

[14] M. Ławniczak, S. Bauch, O. Hul, L. Sirko, *Phys. Scr.* **2009**, 014050 (2009).

[15] M. Ławniczak, S. Bauch, O. Hul, L. Sirko, *Phys. Scr.* **2012**, 014018 (2012).

[16] O. Hul, P. Šeba, L. Sirko, *Phys. Rev. E* **79**, 066204 (2009).

[17] M. Ławniczak, S. Bauch, O. Hul, L. Sirko, *Phys. Scr.* **2011**, 014014 (2011).

[18] M. Ławniczak, M. Białous, V. Yunko, S. Bauch, B. Dietz, L. Sirko, *Acta Phys. Pol. A* **132**, 1672 (2017).

[19] O. Farooq, A. Akhshani, M. Ławniczak, M. Białous, L. Sirko, *Phys. Rev. E* **110**, 014206 (2023).

[20] A. Rehemanjiang, M. Allgaier, C.H. Joyner, S. Müller, M. Sieber, U. Kuhl, H.-J. Stöckmann, *Phys. Rev. Lett.* **117**, 064101 (2016).

[21] J. Lu, J. Che, X. Zhang, B. Dietz, *Phys. Rev. E* **102**, 022309 (2020).

[22] M. Ławniczak, A. Akhshani, O. Farooq, M. Białous, S. Bauch, B. Dietz, L. Sirko, *Phys. Rev. E* **107**, 024203 (2023).

[23] M. Ławniczak, A. Akhshani, O. Farooq, S. Bauch, L. Sirko, *Acta Phys. Pol. A* **144**, 469 (2023).

[24] E. Gutkin, U. Smilansky, *J. Phys. A* **34**, 6061 (2001).

[25] P.B. Kurasov, M. Nowaczyk, *J. Phys. A* **38**, 4901 (2005).

[26] P.B. Kurasov, *Math. Proc. Cambridge Philos. Soc.* **148**, 331 (2010).

[27] R. Band, A. Sawicki U. Smilansky, *J. Phys. A* **43**, 415201 (2010).

[28] O. Hul, M. Ławniczak, S. Bauch, A. Sawicki, M. Kuś, L. Sirko, *Phys. Rev. Lett.* **109**, 040402 (2012).

[29] M. Ławniczak, A. Sawicki, M. Białous, L. Sirko, *Sci. Rep.* **11**, 1575 (2021).

[30] M. Ławniczak, A. Sawicki, S. Bauch, M. Kuś, L. Sirko, *Phys. Rev. E* **89**, 030901 (2014).

[31] R. Band, A. Sawicki, U. Smilansky, *Acta Phys. Pol. A* **120**, A-149 (2011).

[32] O. Farooq, M. Ławniczak, P. Kurasov, L. Sirko, *Sci. Rep.* **15**, 39686 (2025).

[33] M. Ławniczak, P. Kurasov, S. Bauch, M. Białous, V. Yunko, L. Sirko, *Phys. Rev. E* **101**, 052320 (2020).

[34] P.B. Kurasov, *Ark. Mat.* **46**, 95 (2008).

[35] P.B. Kurasov, *J. Funct. Anal.* **254**, 934 (2008).

[36] M. Ławniczak, P. Kurasov, S. Bauch, M. Białous, L. Sirko, *Acta Phys. Pol. A* **139**, 323 (2021).

[37] M. Ławniczak, P. Kurasov, S. Bauch, M. Białous, A. Akhshani, L. Sirko, *Sci. Rep.* **11**, 15342 (2021).

[38] J. Lipovský, *Acta Phys. Pol. A* **128**, 968 (2015).

[39] P. Exner, J. Lipovský, *J. Math. Phys.* **58**, 042101 (2017).